Journal of Alloys and Compounds 592 (2014) 92–99

Contents lists available at ScienceDirect

Journal of Alloys and Compounds

journal homepage: www.elsevier.com/locate/jalcom

The density functional study of electronic structure, electronic charge density, linear and nonlinear optical properties of single crystal alpha-$LiAlTe_2$

A.H. Reshak [a,b], Wilayat Khan [a,*]

[a] New Technologies-Research Center, University of West Bohemia, Univerzitni 8, 306 14 Pilsen, Czech Republic
[b] Center of Excellence Geopolymer and Green Technology, School of Material Engineering, University Malaysia Perlis, 01007 Kangar, Perlis, Malaysia

ARTICLE INFO

Article history:
Received 25 December 2013
Received in revised form 28 December 2013
Accepted 30 December 2013
Available online 9 January 2014

Keywords:
Electronic structure
Electronic charge density
Linear optical properties
Nonlinear optical susceptibilities
DFT

ABSTRACT

Self-consistent calculations is performed using the full potential linear augmented plane wave (FP-LAPW) technique based on density functional theory (DFT) to investigate the electronic band structure, density of states, electronic charge density, linear and non-linear optical properties of α-$LiAlTe_2$ compound having tetragonal symmetry with space group $I\bar{4}2d$. The electronic structure are calculated using the Ceperley Alder local density approach (CA-LDA), Perdew Burke and Ernzerhof generalize gradient approach (PBE-GGA), Engel–Vosko generalize gradient approach (EVGGA) and modified Becke Johnson approach (mBJ). Band structure calculations of (α-$LiAlTe_2$) depict semiconducting nature with direct band gap of 2.35 eV (LDA), 2.48 eV (GGA), 3.05 eV (EVGGA) and 3.13 eV (mBJ), which is comparable to experimental value. The calculated electronic charge density show ionic interaction between Te and Li atoms and polar covalent interaction between Al and Te atoms. Some optical susceptibilities like dielectric constants, refractive index, extension co-efficient, reflectivity and energy loss function have been calculated and analyzed on the basis of electronic structure. The compound α-$LiAlTe_2$ provides a considerable negative value of birefringence of −0.01. Any anisotropy observed in the linear optical properties which are in favor to enhance the nonlinear optical properties. The symbol $\chi^{(2)}_{abc}(\omega)$ represents the second order nonlinear optical susceptibilities, possess six non-zero components in this symmetry (tetragonal), called: 123, 213, 231, 132, 312 and 321 components, in which 123 is the dominant one having value 26.49 pm/V.

1. Introduction

Usually, the ternary chalcogenides having the general formula $A^{I}M^{III}Q_2$ (A = Li, Cu, Ag; M = Al, Ga, In and Q = S, Se, Te) are semiconductor with energy band gaps varying from 0.9 to 4.0 eV [1]. These compounds have got more attenuation due to its optoelectronic relevance's in light emitting diodes (LED), detector, solar energy converters, and nonlinear optical (NLO) tools [2–16]. More often, these (ternary) compounds posses the tetragonal chalcopyrite ($CuFeS_2$) or orthorhombic α-$NaFeO_2$ types of symmetry [17–23]. Both symmetries comprise the tetrahedral building blocks that contribute four corners to contour the three-dimensional meshes; the only disparity is the collapsible series of anions. As a outcome, α-$NaFeO_2$ can be examined as a wurtzite superstructure founded on hexagonal closed collapsible of oxygen, while the chalcopyrite ($CuFeS_2$) structure is considered as a zinc blende (ZnS) superstructure in which sulfur atoms have a cubic closed packing eutaxy.

The majority study has pored on compounds comprising Cu or Ag as the monovalent cation, A^{I}. Very less literature is renowned about ternary lithium chalcogenides possibly because of crystal development adversities and air sensitivity of this class of compounds. This inspired the preparation and characterization of ternary Li-chalcogenides of gallium and indium i.e. $LiGaQ_2$ (Q = S, Se) and $LiInQ_2$ (Q = S, Se, Te), but there is lacking information about the ternary Al-chemistry [22–26]. Though, ternary Li-chalcogenides are very attentive due to their bigger energy band gaps E_g as compared to coinage metal materials and prospectively good for birefringent order materials [24–27]. Due to the wide band gap the ternary Li-chalcogenides possess good attenuation comparable to coinage metal compounds and are eventually appropriate for birefringent crystals [24–27]. Following the structure of these compounds and their similarity to other ternary telluride compounds, one can expect an occurrence of the photoinduced SHG [28].

The Isolated dimmers i.e. $AQ_3 = A_2Q_4Q_{4/2}$ produced due to the sharing of two (AlQ_4) tetrahedral, which are existed in the primary class of materials. The second depicts linear chain $^{1}_{\infty}[AQ_2^- = A_2Q_{4/2}^-]$ formed from the sharing of the edge of tetrahedral AlQ_4 and metals

* Corresponding author. Tel.: +420 775 526 684.
E-mail address: walayat76@gmail.com (W. Khan).

0925-8388/$ - see front matter © 2014 Elsevier B.V. All rights reserved.
http://dx.doi.org/10.1016/j.jallcom.2013.12.251

(alkali) fit within the square anti-prisms between the chains $^{1}_{\infty}[A_2Q_{4/2}^{-}]$.

The last class of the materials prepared from the fusion of diamond like super-tetrahedra $[Al_4Q_{10}]$, possess layers in two co-ordinate $^{1}_{\infty}[A_2Q_6Q_{4/2}^{-}]$, where (Q = Se, Te). Kim and Hughbanks [1] have reported the synthesis and crystal structures of new ternary aluminum chalcogenides, $LiAlSe_2$, α-$LiAlTe_2$, and β-$LiAlTe_2$. During the characteristics of the Telluride compounds it should be emphasized that the electron–phonon interactions play principal role [29].

In the present work, we perform the first principal calculation on α-$LiAlTe_2$ compound using the full potential linear augmented plane wave (FP-LAPW) as employed in the WEIN2K computer program to calculate the band structure, density of states and electronic charge density. We also calculate and completely described the linear/non-linear optical properties of the investigated compound on the basis of the above technique.

The rest of the paper is organized as follow; In Section 2, we briefly describe the computational methodology used in the present work. In Section 3, the principal results like electronic structure, electronic charge density, linear and nonlinear optical susceptibilities are calculated and discussed. Finally, in Section 4, we concluded our results.

2. Computational method

α-$LiAlTe_2$, ternary aluminum chalcogenides having space group $I\bar{4}2d$ with tetragonal symmetry. The unit cell parameters are $a = b = 6.3517$ A°, $c = 11.6904$ A° and $Z = 4$ [1]. The structural diagram of α-$LiAlTe_2$ is displayed in Fig. 1. In this paper, the total energy calculation are performed with the self consistent technique to solve the Kohn–Sham (KS) equations within the framework of density functional theory (DFT) [30,31], using the full potential linearized augmented plane wave (FP-LAPW) method as implemented in the WEIN2K [32] computer package. In the calculation, the converged matrix geometry is determined by using the parameter $R_{MT}K_{MAX} = 7$, where K_{MAX} stands for the plane wave cut off and R_{MT} stand for the minimum of the smallest radii of the atomic sphere. The exchange correlation effects are deal with the local density approach (LDA) [33], generalized gradient approach (GGA) [34], Engel-Vosko generalized gradient approach (EVGGA) [35] and modified Becke Johnson approach (mBJ) [36]. The MT atomic sphere radii are taken to be 2.50 a.u and 2.45 a.u for Li and Al/Te respectively. For stable self consistent calculations, the total energy is in the range of 10^{-3} mRy. Using the Monkhorst–Pack special k-points approximation [37], the integration over the Brillouin zone is carried out up to 405 k-points in the irreducible Brillouin zone (IBZ).

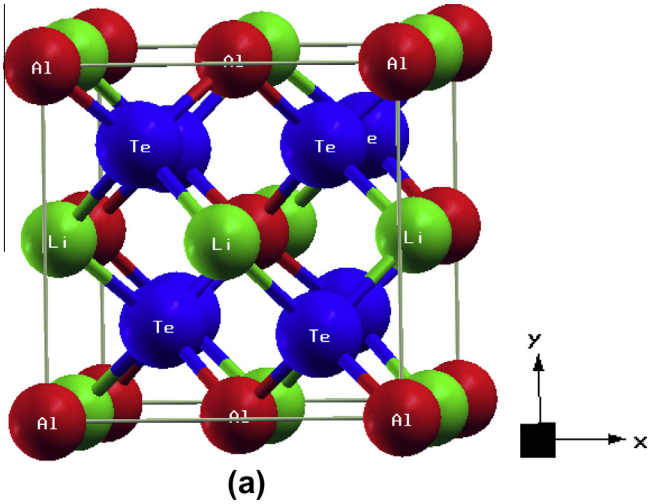

Fig. 1. Crystal structure of, α-$LiAlTe_2$.

3. Result and discussion

3.1. Electronic structure

In order to examine the other properties, we have calculated the electronic band structure of α-$LiAlTe_2$ compound, as illustrated in Fig. 2(a–d). Our calculated band structures depict a direct band gap at Γ-point of BZ. The values of the energy gap are 2.35 eV (LDA), 2.48 eV (GGA), 3.05 eV (EVGGA) and 3.13 eV (mBJ), which is comparable to experimental value [1], as it was mentioned in the introduction that the ternary chalcogenides $A^{I}M^{III}Q_2$ (A = Li, Cu, Ag; M = Al, Ga, In; Q = S, Se, Te) are semiconductors with energy gaps vary between 0.9 and 4.0 eV [1]. Based on this we expected that our calculated band gap using mBJ show reasonable agreement with the experimental value. Therefore we have selected mBJ for further explanation of the other properties i.e. linear and nonlinear optical properties. In the band structure diagram, the lowermost bands are due to the Li-s states and the bands at uppermost part of the valence band arise mainly from Te-p states at Γ-point. The conduction band originates prevailingly from Al-s states exhibiting small energy near Γ the high symmetry point. In order to describe the structure of α-$LiAlTe_2$ compound with more details, we have calculated the total and partial density of states (TDOS and PDOS), as shown in Fig. 3(a–c). Fig. 3a, visualize that the total DOS is shifted toward higher energy along the energy axis, while moving from LDA, GGA, EVGGA and mBJ. The projected DOS of Aluminum (Al), Lithium (Li) and Tellurium (Te) atoms are displayed in Fig. 3(b, c). We divide the valence band into two parts; the first (lower) region start from −11.0 eV to −9.0 eV, which is principally instigating from the Te-p states (localized state) exhibit strong support to partial density of states (3.32 states/eV) and small support provide by Li-s, Al-s and Al-p states to PDOS, respectively. The second part of the valence band lies between −5.1 eV to 0.0 eV (Fermi energy E_F), consist of Li/Al-s, Al/Te-p and Te-d orbital. Among these orbital, we further categorize the orbital into two parts; one is very close to the Fermi energy is originating predominantly from Te-p (quite sharp) and Te-d orbital (relatively localized states) and the second part from Al-s and Al-p respectively. The bottom of the unoccupied band is contributed by the Al-s and Te-p states.

3.2. Electronic charge density

To know more about the distribution of the total electronic charge density maps of α-$LiAlTe_2$ compound, the valence electronic charge density maps has been shown in Fig. 4a along (0 0 1) crystallographic plane. This contour shows that there is no substantial charge density distributed between Li atoms. There is polar covalent character between Al (1.5) and Te (2.1) atoms and the charge transfer occurs mainly from Al atoms towards Te atom due to high electronegativity. It is clear that Te and Li atoms show the ionic nature though the charge density contours around the Te is not completely circular but it shows the ionic bonding nature. The hump appears in the electronic charge density of tellurium atom, due to the high electro negativity which attracts the Al atom. We also calculate the electronic charge density in the (2 1 1) crystallographic plane in order to explore the anisotropy of the electronic charge density in the α-$LiAlTe_2$ compound. As it is clear from Fig. 4b, that in (2 1 1) crystallographic plane, Al atom shows maximum charge density than the Al atom in (0 0 1) plane. In the (2 1 1) plane the Te atom is absent.

3.3. Linear optical properties

Here in this section, we first calculate and analyze the linear optical susceptibilities of the investigated compound α-$LiAlTe_2$

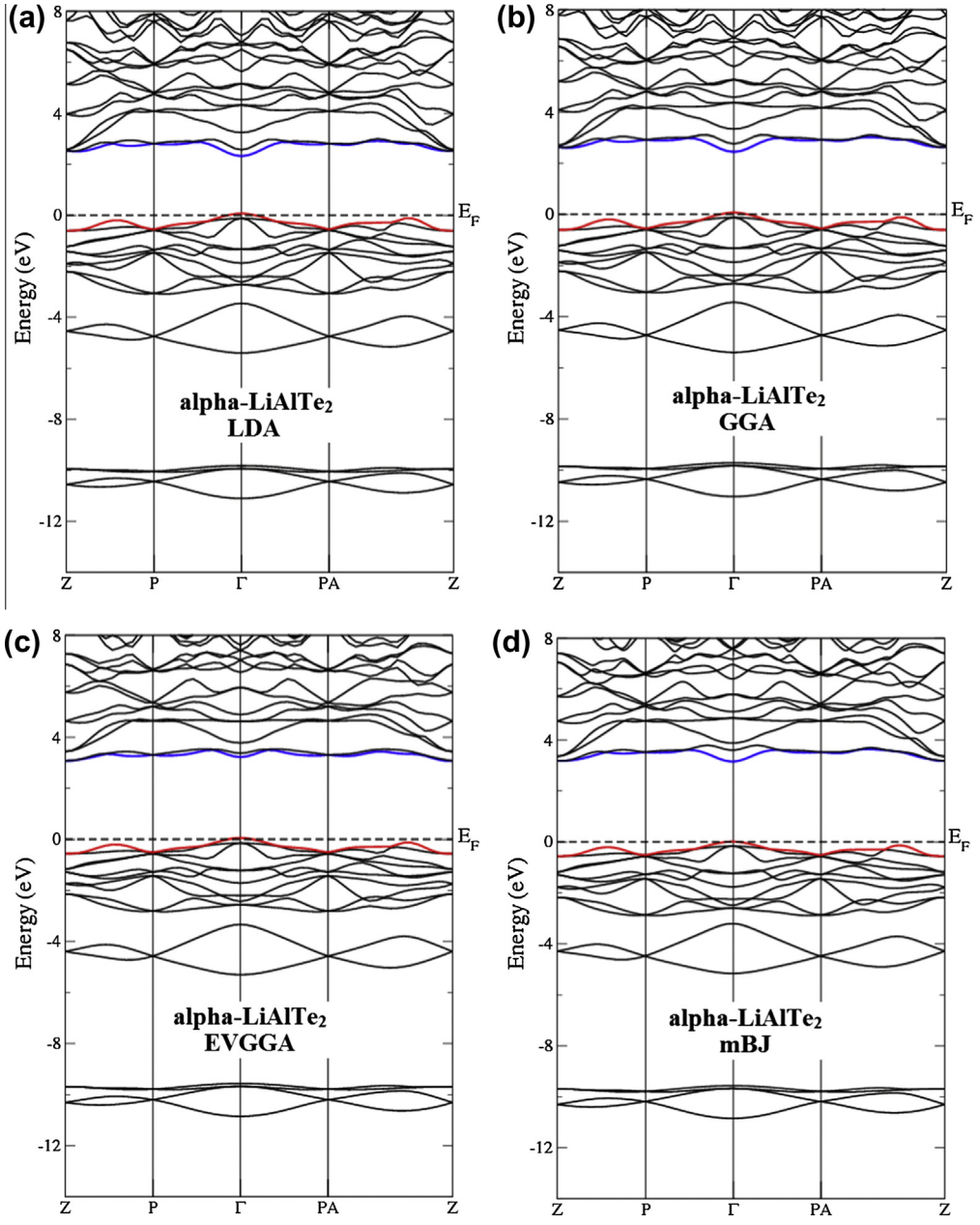

Fig. 2. Calculated band structure of α-$LiAlTe_2$ using LDA, GGA, EVGGA and mBJ.

having tetragonal symmetry, for which we determine only two tensor components ($\varepsilon_2^{xx}(\omega)$ and $\varepsilon_2^{zz}(\omega)$ are major components). These none zero components associated to the parallel and perpendicular parts of the applied electric field to the principle axis, which totally describe the entire linear optical susceptibilities.

The frequency dependent complex dielectric tensor $\varepsilon(\omega)$ components are calculated by using the following mathematical expressions [38,39]:

$$\varepsilon_2^{zz}(\omega) = \frac{12}{m\omega^2}\int_{BZ}\sum\frac{|P_{nn'}^{Z}(k)|^2}{\nabla\omega_{nn'}(k)}\,dS_k \tag{1}$$

$$\varepsilon_2^{xx}(\omega) = \frac{6}{m\omega^2}\int_{BZ}\sum\frac{[|P_{nn'}^{X}(k)|^2 + |P_{nn'}^{Y}(k)|^2]}{\nabla\omega_{nn'}(k)}\,dS_k \tag{2}$$

In the above relations, $e^2 = 1/m = 1$ and $\hbar = 1$ (written in atomic unit)where "ω" is the photon frequency of energy $\hbar\,\omega$, and $P_{nn'}^{X,Y}(k)$ represent the x/y-components of the dipolar matrix elements between initial <nk|(Bra) states and final $|n'k>$ (Ket) states. $\omega_{nn'}(k) =$ Difference in band energies = $E_n(k) - E_{n'}(k)$ (energy eigenvalues), and the last term S_k = constant surface energy = k; $\omega_{nn'}(k) = \omega$. The dispersion spectra of the real $\varepsilon_1(\omega)$ and imaginary $\varepsilon_2(\omega)$ parts of the complex dielectric function $\varepsilon(\omega)$ for relaxed structure of α-$LiAlTe_2$ are indicated in Fig. 5a. The plot of the investigated imaginary part $\varepsilon_2(\omega)$ exposes that the threshold energy appear at 3.13 eV, which is associated to the direct optical transitions from Al-s (Highest valence bands) to Te-p (lowest conduction bands). It is obvious from the Fig. 5a, that there are two main peaks for $\varepsilon_2^{xx}(\omega)$ and $\varepsilon_2^{zz}(\omega)$ in the curve of $\varepsilon_2(\omega)$ along the entire spectral region, located at 5.5 eV and at 5.0 eV (the maximum peak). Following Fig. 5a, one can see that $\varepsilon_2^{zz}(\omega)$ show higher contribution than the *x*-component of $\varepsilon_2(\omega)$. In the energy range from 4.0 eV to 8.0 eV (UV region), both components $\varepsilon_2^{xx}(\omega)$ and $\varepsilon_2^{zz}(\omega)$ indicate considerable anisotropy. The maximum value of the

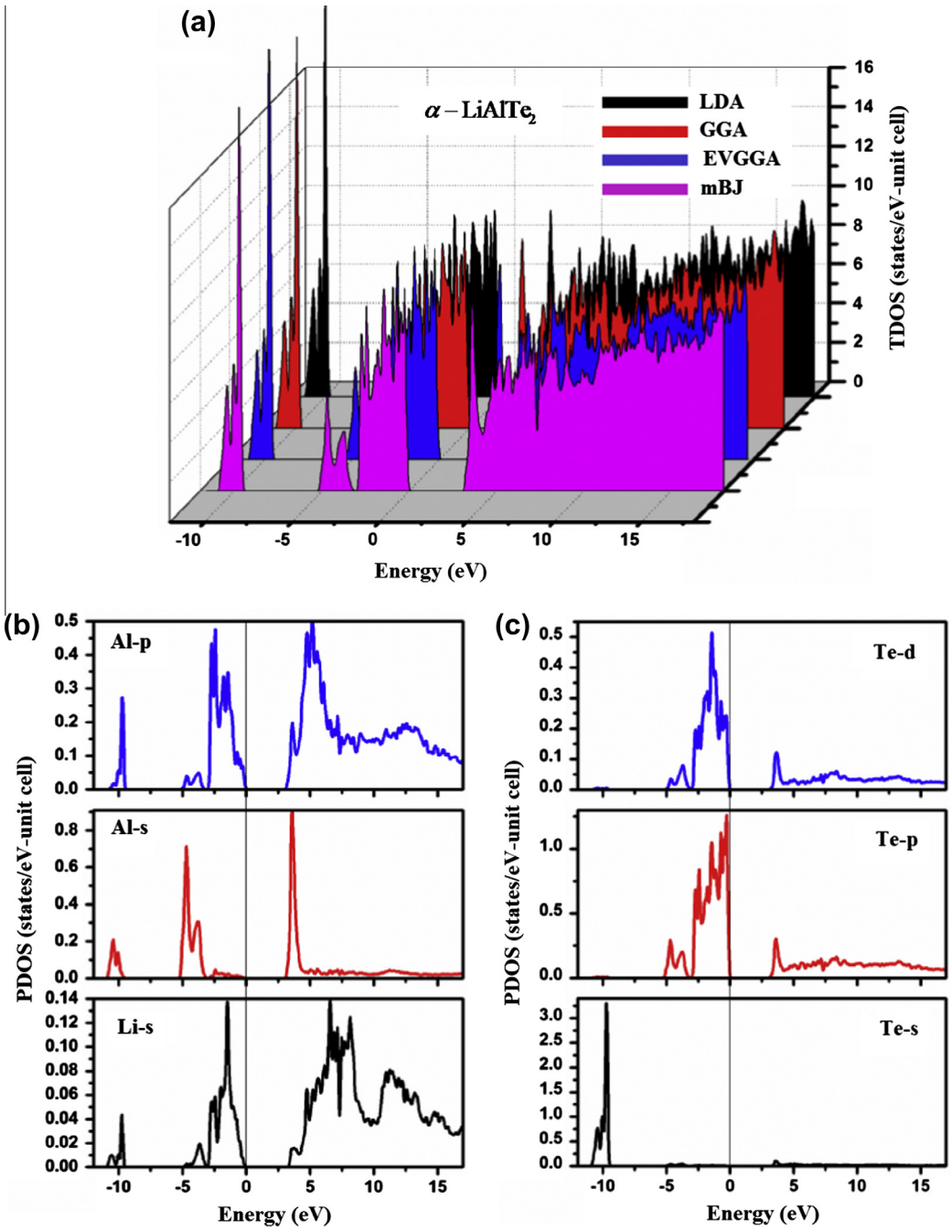

Fig. 3. Calculated total density state (TDOS) and partial density of states (PDOS) of α-$LiAlTe_2$ structure using mBJ.

imaginary part $\varepsilon_2(\omega)$ situated at 5.5 eV is about 12.8, due to the transitions from valence states Al-s to conduction states Te-p. From the dispersion curve (Fig. 5b) of the real part $\varepsilon_1(\omega)$ of the complex dielectric tensor $\varepsilon(\omega)$, we note the static values of $\varepsilon_1(\omega)$ is 5.39 ($\varepsilon_1^{xx}(0)$) and 5.45 ($\varepsilon_1^{zz}(0)$). We should highlight that the smaller value of $\varepsilon_1(0)$ resulted from wide band gap (energy gape), which is inversely proportional to each other. This proportionality could be explained on the basis of Penn model, which is given by; $\varepsilon_1(0) \approx 1 + (h\omega_p/E_g)^2$ [40]. From the Fig. 5b, we observed that $\varepsilon_1(\omega)$ shows the maximum value 10.8 for $\varepsilon_1^{xx}(\omega)$ at 3.7 eV and 12.0 for $\varepsilon_1^{zz}(\omega)$ at 4.0 eV, and some peaks have been observed at 4.5 eV ($\varepsilon_1^{zz}(\omega)$) and 4.9 eV ($\varepsilon_1^{xx}(\omega)$). Above 5.0 eV, the real part $\varepsilon_1(\omega)$ of the dielectric tensor shows decline and reach to lowest peak (−3.0 and −1.8) at 6.1 eV and 8.0 eV for $\varepsilon_1^{xx}(\omega)$ and $\varepsilon_1^{zz}(\omega)$ respectively. By using the expression $\delta\varepsilon = [\varepsilon_0^{II} - \varepsilon_0^{\perp}/\varepsilon_o^{tot}]$, we find uniaxial anisotropy, which is −0.005, proves the anisotropic behavior in the investigated compound α-$LiAlTe_2$.

The calculated frequency dependent refractive index $n(\omega)$ and extension co-efficient $K(\omega)$ are displayed in the Fig. 5(c, d). We note the static values of refractive index $n(\omega)$ is 2.32 ($n^{xx}(0)$) and 2.33 ($n^{zz}(0)$) caused without the lattice oscillation about their mean position i.e. at frequency $\omega = 0$.

We also calculate the birefringence by using the expression, $\Delta n(\omega)$ = difference between the extraordinary and the ordinary refraction indices = $n_e(\omega) - n_0(\omega)$, where $n_0(\omega)$ represents the ordinary refractive index for parallel part of the electric field and $n_e(\omega)$ is the extra ordinary refractive index for the perpendicular part of the electric field along the principal axis. It is obvious that

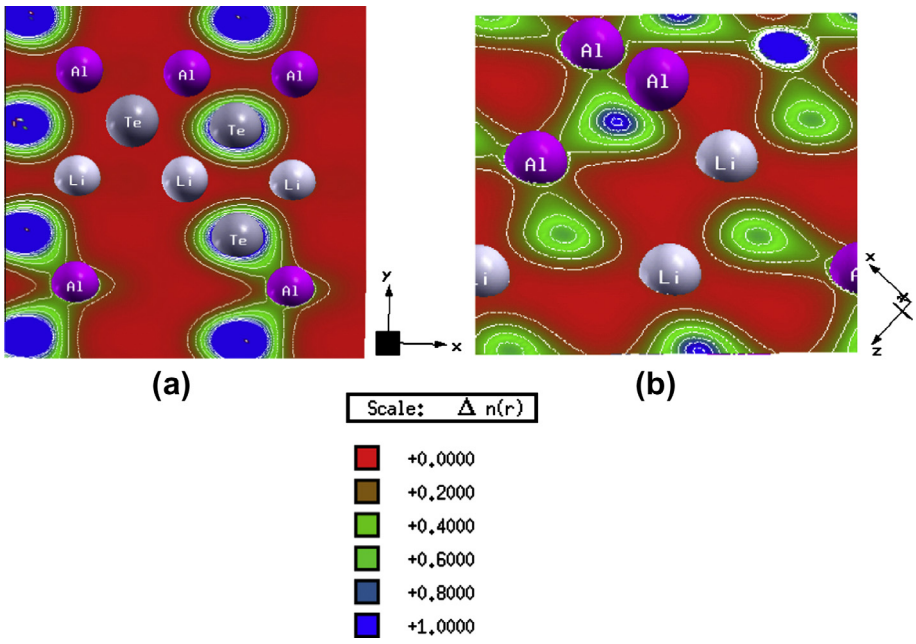

Fig. 4. Electronic space charge density distribution contour calculated with mBJ in the (0 0 1) and (2 1 1) planes of α-$LiAlTe_2$.

below the energy band gap i.e. in the non-absorbing spectral region the birefringence plays an important role. Therefore, the calculated static value of the birefringence $\Delta n(0)$ of the investigated compound is −0.01. The x and y spectral components of refractive index $n(\omega)$ represent highest peaks at energies 3.85 eV and 3.71 eV and the extension co-efficient $k(\omega)$ describes some peaks in the energy range from 4.0 eV to 8.0 eV. While at higher energy both refractive index $n(\omega)$ and extension co-efficient $K(\omega)$ trend to decrease along the spectral region (Fig. 5c and d).

Fig. 5e, shows the plot of reflectivity $R(\omega)$ as a function of frequency ω, which indicates maximum reflectivity 0.65 or 65% at energy about 13.8 eV equal to λ = 89.5 nm (UV region). Consequently, one can say that relax structure of α-$LiAlTe_2$ can be used as a shielding materials regarding to UV radiations. It is clear from the Fig. 5e, that the reflectivity $R(\omega)$ shows anisotropy from 4.0 eV to 13.0 eV.

The energy loss function $L(\omega)$ is very essential factor, which tells exactly about the energy loss of fast electrons traversing into the material. The $L(\omega)$ shows one maximum peak at 13.0 eV and at 13.2 eV, which is associated to the plasma frequency ω_p and the process is called plasma resonance, to which $L(\omega)$ corresponds [41]. Following Fig. 5f, that the energy loss function $L(\omega)$ decreases suddenly, which correlates to the maximum peak occurred in reflectivity and also to the zero crossing of the static value of the refractive index.

3.4. Nonlinear optical properties

In order to explain the calculated second harmonic generation (second order linear optical susceptibility) $\chi^{(2)}_{abc}(-2\omega,\omega,\omega)$ of α-$LiAlTe_2$ correctly we consider the mBJ and quasi-particle self-energy corrections at the level of scissors operators in which the energy bands are rigidly shifted to merely bring the calculated energy gap closer to the experimental gap. The relations for the complex second order nonlinear optical are presented in the previous studies, [42,43]. We can acquire three major contributions from these relations; (1) the inter-band transitions $\chi^{abc}_{\text{inter}}(-2\omega,\omega,\omega)$, (2) the intra-band transitions $\chi^{abc}_{\text{intra}}(-2\omega,\omega,\omega)$ and (3) $\chi^{abc}_{\text{mod}}(-2\omega,\omega,\omega)$ are the modulation of inter-band by intra-band terms. Mathematically, all these three terms can be expressed as:

$$\chi^{abc}_{\text{inter}}(-2\omega,\omega,\omega)=\frac{e^3}{\hbar^2\Omega}\sum_{nml,k}\frac{r^a_{nm}\{r^b_{ml}r^c_{\text{ln}}\}}{(\omega_{\text{ln}}-\omega_{ml})}\left[\frac{2f_{nm}}{\omega_{mn}-2\omega}+\frac{f_{\text{ln}}}{\omega_{\text{ln}}-\omega}+\frac{f_{ml}}{\omega_{ml}-\omega}\right] \tag{3}$$

The term $\chi^{abc}_{\text{inter}}(-2\omega,\omega,\omega)$ = is mainly from the inter-band contribution with $\{r^b_{ml}r^c_{\text{ln}}\}=(1/2)(r^b_{ml}r^c_{\text{ln}}+r^c_{ml}r^b_{\text{ln}})$ and n,m,l stands for the different band indices.

$$\chi^{abc}_{\text{intra}}(-2\omega;\omega,\omega)=\frac{e^3}{\hbar^2}\int\frac{d\vec{k}}{4\pi^3}\left[\sum_{nml}\omega_{nm}\vec{r}^{\,i}_{nm}\{\vec{r}^{\,j}_{ml}\vec{r}^{\,k}_{ln}\}\right.$$
$$\left\{\frac{f_{nl}}{\omega^2_{ln}(\omega_{ln}-\omega)}-\frac{f_{lm}}{\omega^2_{ml}(\omega_{ml}-\omega)}\right\}-8i\sum_{nm}\frac{f_{nm}\vec{r}^{\,i}_{nm}\{\Delta^j_{mn}\vec{r}^{\,k}_{nm}\}}{\omega^2_{mn}(\omega_{mn}-2\omega)}$$
$$\left.+2\sum_{nml}\frac{f_{nm}\vec{r}^{\,i}_{nm}\{\vec{r}^{\,j}_{ml}\vec{r}^{\,k}_{ln}\}(\omega_{ml}-\omega_{ln})}{\omega^2_{mn}(\omega_{mn}-2\omega)}\right] \tag{4}$$

$$\chi^{abc}_{\text{mod}}(-2\omega;\omega,\omega)=\frac{e^3}{2\hbar^2}\int\frac{d\vec{k}}{4\pi^3}\left[\sum_{nml}\frac{f_{nm}}{\omega^2_{mn}(\omega_{mn}-\omega)}\{\omega_{nl}\vec{r}^{\,i}_{lm}\{\vec{r}^{\,j}_{mn}\vec{r}^{\,k}_{nl}\}\right.$$
$$\left.-\omega_{lm}\vec{r}^{\,i}_{nl}\{\vec{r}^{\,j}_{lm}\vec{r}^{\,k}_{mn}\}\}-i\sum_{nm}\frac{f_{nm}\vec{r}^{\,i}_{nm}\{\vec{r}^{\,j}_{mn}\Delta^k_{mn}\}}{\omega^2_{mn}(\omega_{mn}-\omega)}\right] \tag{5}$$

The first two terms in the above equation consist of the modified linear response caused by the intra-band transitions and the last two term intra-band term is varied by a phenomenon, called the polarization of inter-band. The energy difference between the upper- band n and lower band m, and the Fermi distribution functions can be written as $\hbar\omega_{mn}=\hbar\omega_n-\hbar\omega_m$, and $f_{mn}=f_n-f_m$. The terms a, b and c are the Cartesian indices, from which we calculate the unit cell volume, and ω = frequency = $\omega+i\delta$, where δ (delta function → 0). Generally, the symbol r stands for the position operator. Despite of ω, all the terms depends on the k (vector space), and the generalized co-ordinates of vector space can be expressed as $r^b_{nm:a}$. Where Δ^b_{nm} stands for the variation between the velocities of electrons at n and m bands $=p^a_{nn}-p^a_{mm}/m$. The above equations are already compact to a shape displaying single ω or 2ω resonances, slightly than combinations of two such energy denominators that facilitate us to calculate the imaginary part and real part by using the Kramer–Kronig relation, separately. $r^a_{nm}(k)$, stands for

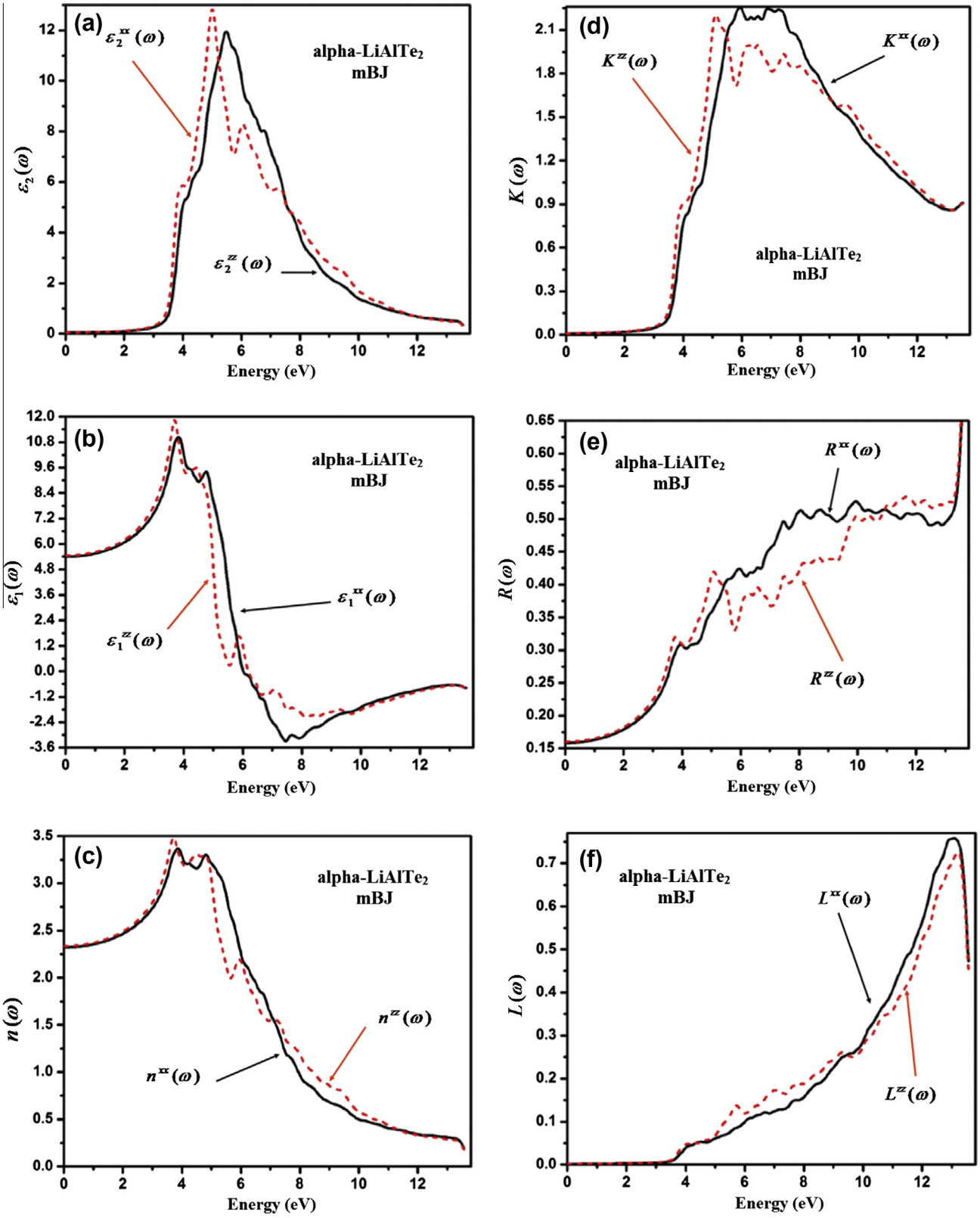

Fig. 5. Calculated real and imaginary part of dielectric function, reflectivity, refractive index, extension co-efficient and energy loss function of α-$LiAlTe_2$ using mBJ.

the position matrix elements between n and m bands, are obtained from the momentum matrix element $p^a_{nm}(k)$, using the expression [44], $r^a_{nm}(k) = \frac{p^a_{nm}(k)}{im\omega_{nm}(k)}$.

Aspnes [45] verified that only transitions from one occupied states to two unoccupied states, known as virtual-electron transitions, give a major support to the second order tensor components. Therefore we disregard as it was discovered to be negative and more than an alignment of magnitude lesser than the virtual-electron role for these compounds. Simply we represent $\chi^{(2)}_{abc}(-2\omega,\omega,\omega)$ by $\chi^{(2)}_{abc}(\omega)$.

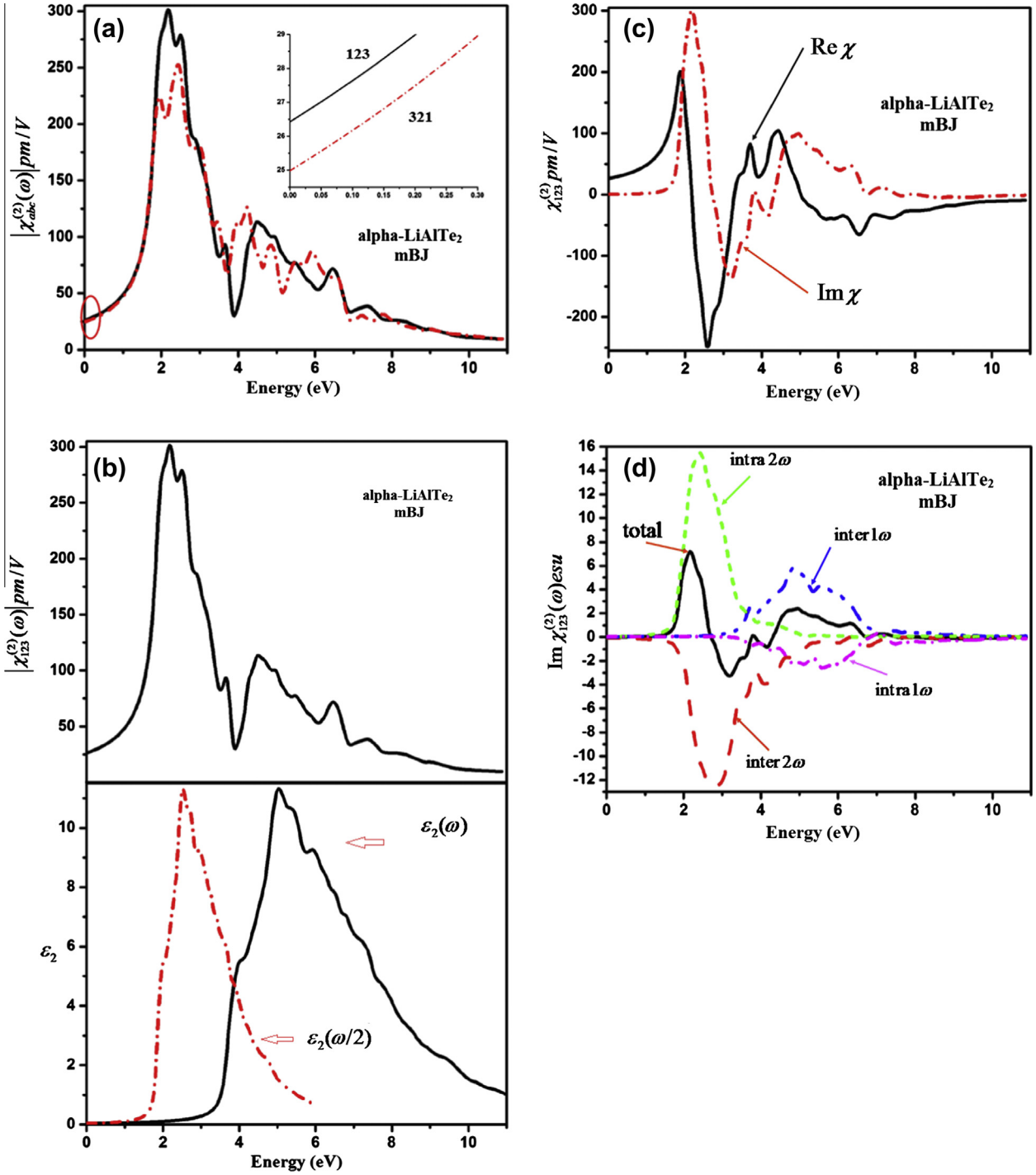

Fig. 6. Calculated non linear optical properties compound of α-$LiAlTe_2$.

We have calculated the second order susceptibilities of the investigated crystals α-$LiAlTe_2$ having point group $I\bar{4}2d$. There are six non-zero independent tensor components of the second harmonic generation (SHG), called: 123, 213, 231, 132, 312 and 321 components (1, 2, and 3 refer to the x, y and z axes, respectively) [46]. As the first four components are equal i.e. 123 = 213 = 231 = 132 and the last two are equal too i.e. 321 = 312, therefore we have plotted only 123 and 321 components. We should accentuate that the nonlinear optical properties are more perceptive as compared to the linear optical properties due to the minor changes of band structure.

The calculated absolute value of the second harmonic tensor $|\chi^{(2)}_{abc}(\omega)|$ for 123 and 321 components, describe that the component $|\chi^{(2)}_{123}(\omega)|$ shows dominancy than $|\chi^{(2)}_{321}(\omega)|$, as the component $|\chi^{(2)}_{123}(\omega)|$ possesses greater static values (26.42) at $\omega = 0$ as compared to $|\chi^{(2)}_{321}(\omega)|$ (see Fig. 6a).

It would be very useful to compare the absolute value of the principal component $|\chi^{(2)}_{123}(\omega)|$ with the imaginary part of the complex dielectric function $\varepsilon_2(\omega)$ and $\varepsilon_2(\omega/2)$ as displayed in the Fig. 6b. Following Fig. 6b, the first part of the spectra of $|\chi^{(2)}_{123}(\omega)|$ lies from 1.94 eV to 3.7 eV is mainly appearing due to the 2ω resonance. The second part of the spectra, which lies above 3.7 eV till

5.0 eV, corresponds to the major contribution of the ω and 2ω resonance. The last spectral structure (within 5.0 – 10.0 eV) is mainly due to ω resonance and is associated with the second structure in $\varepsilon_2(\omega)$.

Fig. 6c, depicts the calculated complex part of the second harmonic susceptibility of the investigated compound α-$LiAlTe_2$. It has been observed that less than half of the band gap, the total nonlinear optical susceptibilities acquiring SHG is equal to zero. At energy equal to $1/2E_g$, the frequency 2ω begins to contribute and the term having the frequency ω begins to contribute above E_g (energy band gap). In the energy range below 3.26 eV, the SHG spectrum is mainly from the 2ω supports. The frequency ω term provide main support at energy greater than 3.26 eV (value of the fundamental band gap). It is obvious from the Fig. 6c, that the coefficient $\chi^{(2)}_{123}(\omega)$ of SHG is considerable along the whole range of the photon energy $\hbar\omega$. In addition, $\chi^{(2)}_{123}(\omega)$ is entirely in dispersive form in the small energy range of photon.

The calculated imaginary parts of the second harmonic generation (SHG) is plotted as a function of photon energy $\hbar\omega$, as shown in the Fig. 6c. We take the Krammers–Kronig integral relation, which is given as:

$$\mathrm{Re}[\chi^{(2)}_{123}(0,0,0)] = (2/\pi)p\int_0^\infty \{\mathrm{Im}[\chi^{(2)}_{123}(-2\omega,\omega,\omega)]/\omega\}\,d\omega \qquad (6)$$

Using the above relation, we derive the static values at frequency $\omega = 0$. The second harmonic generation also approaches to zero very rapidly at higher energy above 7.0 eV. These details can be used in the prospect for molecular engineering of the crystals in the enviable directions. We suggest that the calculated data may act as a dominant tool for more design of the crystals with the better SHG properties. Additionally, one can examine different factors in SHG from the investigation of frequencies ω and 2ω due to the putrefaction of separate band to band supports same to the investigation of linear optical susceptibilities. Fig. 6d, exposes 2ω inter/intra band as well as 1ω inter/intra band support to the imaginary part of the nonlinear optical susceptibilities $\chi^{(2)}_{123}(\omega)$ components. One can clearly note the variation of signs due to the above contributions along the entire range of frequency.

4. Conclusions

In conclusion, the linear and nonlinear optical susceptibilities of nonlinear α-$LiAlTe_2$ compound are calculated using the density functional theory based on the full potential linear augmented plane wave (FP-LAPW) technique. Our calculated band structure of the investigated compound exhibits direct band gape of about 2.35 eV (LDA), 2.48 eV (GGA), 3.05 eV (EVGGA) and 3.13 eV (mBJ), which is comparable to experimental value. The analyzed densities of states indicate strong contribution from Te-p states close to the Fermi level E_F, which plays a significant role in the optical properties. Our calculated electronic charge density contours show the polar covalent bond between Al and Te atoms, and ionic bond between Li and Te atoms, respectively. We calculate the linear optical properties like real and imaginary part of the dielectric tensor, reflectivity, refractive index, extension co-efficient and energy loss function on the basis of electronic structure. Our calculated results for linear optical susceptibilities show maximum reflectivity (65%) in the ultra violet region, which describe that the compound α-$LiAlTe_2$ can be used as shielding materials. Our calculated birefringence possesses considerable negative value of −0.01, which plays an important role in the non-absorbing spectral region below the energy band gap. We also calculate the second order nonlinear optical properties, in which we find that $\chi^{(2)}_{123}(\omega)$ component is dominant than those having co-ordinate indices namely: 123, 213, 231, 132, 312 and 321 respectively, in which the first four (123, 213, 231, 132) and the last two (312, 321) components are equal. We observed that any anisotropic behavior is observed in linear optical properties increases the nonlinear optical susceptibilities. Our results depict that the 2ω inter/intra-band contributions to the real and imaginary parts of $\chi^{(2)}_{123}(\omega)$, which are influenced by signs. These details can be used in the prospect for molecular engineering of the crystals in the enviable directions.

Acknowledgements

This result was developed within the CENTEM project, reg. no. CZ.1.05/2.1.00/03.0088, co-funded by the ERDF as part of the Ministry of Education, Youth and Sports OP RDI program.

References

[1] J. Kim, T. Hughbanks, Inorg. Chem. 39 (2000) 3092–3097.
[2] C. Rincón, S.M. Wasim, G. Marın, J.R. Huntzinger, J. Galibert, A. Zwick, Mater. Lett. 38 (1999) 305–307.
[3] C. Rincón, E. Hernandez, S.M. Wasim, I. Molina, J. Phys. Chem. Solids 56 (1998) 1015–1019.
[4] Marın, G.C. Rincón, S.M. Wasim, C. Power, G.S. Peréz, J. Appl. Phys. 81 (1997) 7580–7583.
[5] H.S. Soliman, J. Phys. D: Appl. Phys. 31 (1998) 1516–1521.
[6] D.J. Bottomley, A. Mito, S. Niki, A. Yamada, J. Appl. Phys. 82 (1997) 817–824.
[7] D.J. Bottomley, A. Mito, P.J. Fons, S. Niki, A. Yamada, IEEE J. Quantum Electron. 33 (1997) 1294–1298.
[8] A.G. Jackson, M.C. Ohmer, S.R. LeClair, Infrared Phys. Technol. 38 (1997) 233–244.
[9] Q.B. Meng, C.Y. Xiao, Z.J. Wu, K.A. Feng, Z.D. Lin, S.Y. Zhang, Solid State Commun. 107 (1998) 369–371.
[10] G. Brandit, A. Räuber, J. Schneider, Solid State Commun. 12 (1973) 481–483.
[11] M. Robbins, V.G. Lambrecht Jr., Mater. Res. Bull. 8 (1973) 703–710.
[12] V.G. Lambrecht Jr., Mater. Res. Bull. 8 (1973) 1383–1388.
[13] M. Robbins, J.C. Phillips, V.G. Lambrecht Jr., J. Phys. Chem. Solids. 34 (1973) 1205–1209.
[14] M. Robbins, V.G. Lambrecht Jr., J. Solid State Chem. 15 (1975) 167–170.
[15] G.D. Boyd, H.M. Kasper, J.H. McFee, J. Appl. Phys. 44 (1973) 2809–2812.
[16] T.J. Negran, H.M. Kasper, A.M. Glass, Mater. Res. Bull. 8 (1973) 743–748.
[17] R. Hoppe, Bull. Soc. Chim. Fr. (1965) 1115–1121.
[18] V.H. Hahn, G. Frank, W. Klingler, A.D. Meyer, G.Z. Störger, Anorg. Allg. Chem. 271 (1953) 153–170.
[19] S.C. Abrahams, J.L. Berstein, J. Chem. Phys. 59 (1973) 1625–1629.
[20] S.C. Abrahams, J.L. Berstein, J. Chem. Phys. 59 (1973) 5415–5422.
[21] S.C. Abrahams, J.L. Berstein, J. Chem. Phys. 61 (1974) 1140–1146.
[22] W. Hönle, G. Kühn, H.Z. Neumann, Anorg. Allg. Chem. 532 (1986) 150–156.
[23] W. Hönle, G. Kühn, H.Z. Neumann, Anorg. Allg. Chem. 543 (1986) 161–168.
[24] T. Kamijoh, K. Kuriyama, J. Cryst. Growth 46 (1979) 801–803.
[25] K. Kuriyama, T. Nozaki, J. Appl. Phys. 52 (1981) 6441–6443.
[26] T. Kamijoh, T. Nozaki, J. Cryst. Growth 51 (1981) 6–10.
[27] K. Kuriyama, T. Nozaki, J. Appl. Phys. 52 (1981) 1102–1103.
[28] K. Nouneh, I.V. Kityk, R. Viennois, S. Benet, K.J. Plucinski, S. Charar, Z. Golacki, S. Paschen, J. Phys. D: Appl. Phys. 38 (2005) 965–973.
[29] H. Kaddouri, S. Benet, S. Charar, M. Makowska-Janusik, J.C. Tedenac, Phys. Rev. B. 62B (24) (2000) 17108–17116.
[30] P. Younbong et al. 257 (1997) 137–145.
[31] P. Hohenberg, W. Kohn, Phys Rev 136 (1964) 684.
[32] P. Balaha, K. Shewartz, G.K.H. Madsen, D. Kvsnicka, J. Luitz, WIEN2K, an Augmented Plane Wave + local Orbitals Program for Calculating Crystals Properties, Karlheinz Schewartz, Universitat, Wien Austria, Techn, 2001, ISBN 3-9501031-1-2.
[33] J.P. Perdew, Y. Wang, Phys. Rev. B 45 (1992) 13244.
[34] J.P. Perdew, J.A. Chevary, S.H. Vosko, K.A. Jackson, M.R. Pederson, D.J. Singh, C. Fiolhais, Phys. Rev. B 46 (1992) 6671.
[35] E. Engel, S.H. Vosko, Phys. Rev. B 47 (1993) 13164;
E. Engel, S.H. Vosko, Phys. Rev. B 50 (1993) 10498.
[36] F. Tran, P. Blaha, Phys. Rev. Lett. 102 (2009) 226401–226405.
[37] H.J. Monkhorst, J.D. Pack, Phys Rev B 13 (1976) 5188.
[38] A.H. Reshak, S. Auluck, Phys Rev B. 68 (2003) 245113.
[39] S. Sharma, S. Auluck, M.A. Khan Pramana, J. Phys. 54 (1999) 431.
[40] D.R. Penn, Phys. Rev. B 128 (1962) 2093.
[41] O.L. Anderson, J. Phys. Chem. Solids 24 (1963) 909.
[42] S. Sharma, J.K. Dewhurst, C. Ambrosch-Draxl, Phys Rev B 67 (2003) 165332.
[43] A.H. Reshak, S. Auluck, A. Majchrowski, I.V. Kityk, PMC Phys. B 1 (2008) 8.
[44] C. Ambrosch-Draxl, J.O. Sofo, Comput. Phys. Commun. 175 (2006) 1.
[45] D.E. Aspnes, Phys. Rev. B 6 (1972) 4648.
[46] W. Boyd, Nonlinear Optics Academic Press, Boston, 1992.